Ollscoil na Gaillimhe
University of Galway

Provided by the author(s) and University of Galway in accordance with publisher policies. Please cite the published version when available.

Title	Pyrolysis of n-pentane, n-hexane and n-heptane in a single pulse shock tube
Author(s)	Yasunaga, Kenji; Yamada, Hiroshi; Oshita, Hidekazu; Hattori, Kenji; Hidaka, Yoshiaki; Curran, Henry J.
Publication Date	2017-08-16
Publication Information	Yasunaga, Kenji, Yamada, Hiroshi, Oshita, Hidekazu, Hattori, Kenji, Hidaka, Yoshiaki, & Curran, Henry. (2017). Pyrolysis of n-pentane, n-hexane and n-heptane in a single pulse shock tube. Combustion and Flame, 185, 335-345. doi: 10.1016/j.combustflame.2017.07.027
Publisher	Elsevier
Link to publisher's version	https://doi.org/10.1016/j.combustflame.2017.07.027
Item record	http://hdl.handle.net/10379/14791
DOI	http://dx.doi.org/10.1016/j.combustflame.2017.07.027

Downloaded 2024-05-11T04:36:02Z

Some rights reserved. For more information, please see the item record link above.

Pyrolysis of *n*-pentane, *n*-hexane and *n*-heptane in a single pulse shock tube

KENJI YASUNAGA[1*], HIROSHI YAMADA[1], HIDEKAZU OSHITA[2], KENJI HATTORI[2], YOSHIAKI HIDAKA[2], HENRY CURRAN[3]

[1]Department of Applied Chemistry, National Defense Academy, Yokosuka, Japan

[2]Chemistry and Biology, Graduate School of Science and Engineering, Ehime University, Matsuyama, Japan

[3]Combustion Chemistry Centre, School of Chemistry, National University of Ireland, Galway, Ireland

Corresponding Author: Email address: yasunaga@nda.ac.jp (KENJI YASUNAGA)

Abstract

The pyrolysis of *n*-pentane, *n*-hexane and *n*-heptane have been studied behind reflected shock waves at pressures of 1.0–2.5 atm and at temperatures of 1000–1500 K. A single-pulse shock tube (SPST) was used to measure reactant, intermediate, and product species profiles using GC samplings at different reaction times varying from 1.5 to 2.2 ms. Simulations have been performed using two chemical kinetic models for the three fuels, namely NUI Galway and JetSurf (Version2.0). Differences in simulated results between the models are described. Sensitivity and reaction path analyses were performed to determine the important reactions controlling fuel pyrolysis and their influence on the predicted concentrations of reactant and product species profiles compared to those measured in the experiments.

1. Introduction

A dramatic reduction in the cost of launching space vehicles is necessary for the promotion of space utilization. Expensive rocket engines and fuel tanks are currently dumped into the ocean without reuse. The Japan Aerospace Exploration Agency (JAXA) has proposed a winged reusable space vehicle [1] which consists of a rocket engine and an air-breathing ramjet engine termed the Rocket-Based-Combined-Cycle (RBCC) engine. Since the ramjet combustion chamber is exposed to the rocket exhaust heat on the structure, a cooling and thermal protection system needs be employed. A regenerative cooling system uses fuels as coolants. These flow through channels in the walls of the combustion chamber prior to their injection into it. Liquefied hydrogen (LH_2) and hydrocarbons are considered as fuels for RBCC engines. LH_2 has advantages as a coolant and as a fuel due to its average specific heat and heat of combustion; however, it costs more than hydrocarbons and requires huge tanks due to its low density. Hydrocarbon fuels undergo pyrolysis which is an endothermic reaction at high temperatures, which works as an additional chemical heat sink. The composition of hydrocarbon fuels varies during pyrolysis from the original, which results in a mixture of low- and higher-order hydrocarbons. *n*-Pentane is the smallest straight-chained alkane that exists in the liquid phase at normal conditions of pressure and temperature. Sajid et al. [2] performed shock tube/laser absorption measurements using quantum cascade and CO_2 lasers to monitor concentrations of methane, acetylene and ethylene during the pyrolysis of *n*-pentane. Westbrook et al. [3] monitored chemical species using a well-stirred reactor in the oxidation of *n*-pentane at 1 atm and at

temperatures ranging from 1068 to 1253 K. Gonzalez and Sandler [4] used an annular flow reactor to study the oxidation of *n*-pentane at 1 atm and monitored the products using gas chromatography and other methods in the temperature range 793–893 K.

Mével et al. [5] used a flow reactor to measure the gas phase mixture composition of *n*-hexane oxidation by both laser-based diagnostics and gas chromatography at low temperature and at 1 bar. The low temperature oxidation of the five hexane isomers was investigated by Wang et al. [6] in a jet-stirred reactor (JSR) between 550–1000 K at 1 atm. Intermediate species concentrations were measured using both gas chromatography mass spectrometry (GC-MS) and synchrotron vacuum ultraviolet photoionization mass spectrometry (SVUV-PIMS) techniques [7]. Zhang et al. [8] measured concentration including reactant and intermediates during the oxidation of *n*-hexane in a jet-stirred reactor over a wide range of temperature (530–1160 K) at 10 atm.

Numerous experimental works for species versus time and/or temperature profiles in the *n*-heptane oxidation have been performed in jet-stirred reactors [9-13] and flow reactors [14-16]. Chakir et al. [9] measured species concentrations for the oxidation of *n*-heptane in a JSR in the temperature range 950-1200 K and at 1 atm for a wide range of fuel-oxygen equivalence ratios (0.2 to 2.0). *n*-Heptane and *iso*-octane oxidation has been studied by Dagaut et al. measuring the concentrations of reactants and products in a high pressure JSR covering a wide temperature range of 550–1150 K at 10 atm [10] and 1–40 atm [11]. The low temperature oxidation of *n*-heptane was investigated by Herbinet et al. [12] in a JSR in the temperature range 500–1100 K at pressures in the range 1–40 atm using both gas

chromatography and SVUV-PIMS techniques. Hakka et al. [13] investigated ultra rich fuel oxidation of *n*-heptane measuring 24 intermediates by GC-MS in a JSR ranging from 550–1100 K at a pressure of 1.06 bar and at an equivalence ratio of 3. The oxidation of *n*-heptane and *iso*-octane oxidation was also studied in a pressurized flow reactor by Callahan et al. [14] measuring the concentrations of reactants, oxygen molecule and final products (CO_2,CO and H_2) covering a temperature range of 550–900 K at 12.5 atm. Species concentration profiles of reactants and several intermediates were measured for *n*-heptane oxidation in a flow reactor over the low and intermediate temperature regime (600–800 K) at 8 atm by Lenhert et al. [16]. Held et al. [17] performed an experimental study of *n*-heptane pyrolysis and oxidation in a variable pressure flow reactor measuring reactant and products concentrations at temperatures of 940, 1075 and 1085 K and at a pressure of 3 atm. Several studies for measuring species concentrations have been performed for *n*-pentane, *n*-hexane and *n*-heptane as described above. However, concentration profiles for the pyrolysis of these compounds are very limited. Species concentration profiles using GC sampling including reactants and products resulted from the pyrolysis of *n*-pentane, *n*-hexane and *n*-heptane have been measured in a single-pulse shock tube (SPST) and are compared with simulations in this study.

2. Experimental Section

Samples of *n*-pentane, *n*-hexane and *n*-heptane fuels 99.0%, 96.0% and 99.0% pure were supplied by Kanto Kagaku and Hayashi Junyaku, and degassed through a series of

freeze-thaw-pump cycles, after which no more gas was observed to escape on thawing the solid. Argon (99.999% pure) was supplied by Teisan Co. and Iwatani. Mixtures were prepared using the method of partial pressures. The incident shock velocity was used to calculate the temperatures and pressures of the mixtures behind the reflected shock wave using the equilibrium program Gaseq [18]. All shock temperatures and pressures were calculated from the measured incident shock velocity assuming full vibrational relaxation with no chemical reaction. These temperatures and pressures were used for all figures. The single-pulse-shock-tube (SPST) of 4.1 cm i.d. used in this study has a magic-hole in the low-pressure section. A simple description is only given below, since the apparatus has been described in detail previously by Hidaka et al [19-22]. The reacted gas mixtures were quenched using the single pulse method. They were then extracted into a pre-evacuated vessel (50 cm^3) and were analyzed using three serially connected gas chromatographs, each having a thermal conductivity detector (TCD) [21,22]. The gas chromatographic analyses were carried out as follows. A Shimadzu GC-8A with 2 m column packed with Sebaconitrile and heated to 75 ^oC was used to determine the concentrations of hydrocarbons above C_4. A Shimadzu GC-8A with 2 m column packed with Porapak Q connected to a 2 m column packed with Unibeads 1S was used to determine the concentrations of C_2 and C_3 hydrocarbons. These columns were heated at a rate of 3 ^oC/min from 50 to 130 ^oC. A Shimadzu GC-8A with 2 m column packed with Molecular Sieve 5 A at 50 ^oC was used to determine the concentration of CH_4. Helium was used as the carrier gas. The output signal from each gas chromatograph was introduced into Shimadzu Chromatopac C-R3A-1,

C-R3A-2 data processors. An effective heating time, t_e (reaction time), which was defined as the time between the arrival of the reflected shock pressure and when it had fallen by 20%, was determined with an accuracy of ±5% using the method described previously [20,21]. Assuming adiabatic expansion of the non-reactive mixtures, the temperature drops by 8.5% from its initial value at the effective heating time. The calibration method used in the GC analysis to estimate the concentrations of reactants and products is briefly described here. The sensitivities of the detector to each species were determined using the peak area of known species concentrations. These sensitivities are normalized against argon as the standard. The concentrations of species as a result of shock heating are estimated using the sensitivity together with the measured area ratios and the known argon concentration. The details of this method are described in Chapter 6 of [23].

Given that single pulse shock tubes have cooling rates of 6.6×10^5 K s^{-1}[19], it can be assumed that the reaction was frozen at the effective heating time, the concentrations of carbon containing compounds, determined by gas chromatography, were compared with those from the simulations. The validity of the effective heating time and cooling rate was previously tested for N_2O pyrolysis [19]. The estimated uncertainty in the measured temperatures, species concentrations and effective heating times are 1%, 8% and 5%, respectively.

3. Model and Simulation

Simulations were performed with Chemkin-Pro [24], using the closed homogeneous batch reactor model at constant volume for our shock tube experiments.

Previous modeling studies at the National University of Ireland Galway (NUIG) for *n*-pentane [25], *n*-hexane [8] and *n*-heptane [26] oxidation have been published covering a wide variety of reactors and conditions. However, the isomerization of 1-heptyl radicals to 3-heptyl radicals via a 6-membered transition state ring is not included in the previously published *n*-heptane model [26]. Isomerization reactions and rate constants of hexyl and heptyl radicals in the NUIG model are updated based on the recent work of Sirjean et al. [27] and used in our simulations. JetSurF (version2.0) [28] is a chemical kinetic model constructed for the high temperature oxidation including *n*-alkanes up to *n*-dodecane. Both models from NUIG [8,25,26] and JetSurF (version 2.0) [28] were used to simulate species concentration profiles obtained in this work, and the differences between the two models are discussed in the latter part of this paper. The reactions and reaction numbers influencing the concentrations of reactant and product species are discussed based on the NUIG model.

Comparison to Experiment

n-Pentane

The species profiles were measured using SPST and simulated for three mixtures of 1.6% *n*-pentane, 0.4% *n*-hexane and 1.0% *n*-heptane diluted in argon respectively in the pressure range 1.0–2.5 atm with effective heating times in the range of 1.5–2.2 ms. Effective heating

times decrease as the shock velocity increases, which results in higher temperatures. Hence, heating times decrease as the temperature increases. The results of *n*-pentane pyrolysis are shown in Fig. 1.

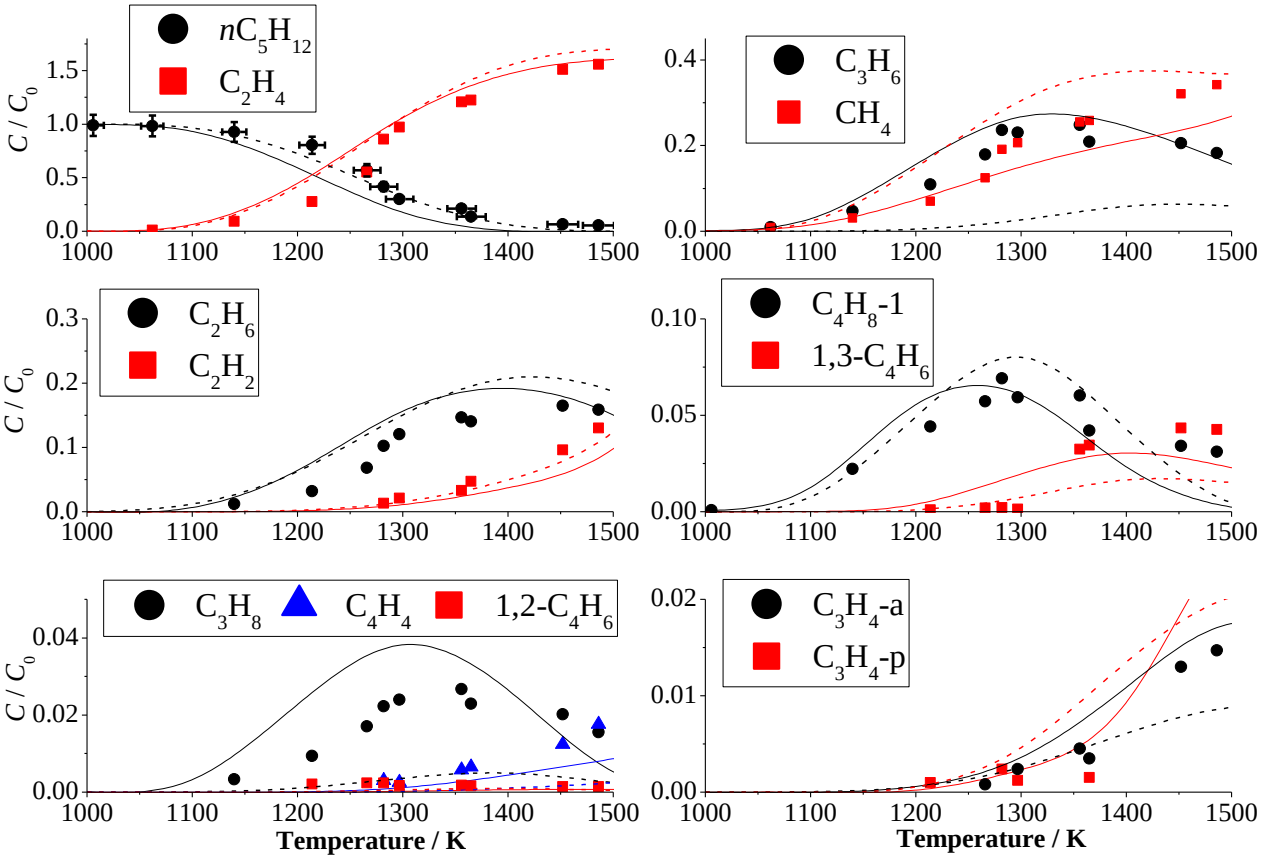

Fig. 1. Species profiles from SPST for 1.6% *n*-pentane diluted in Ar at 1.2-2.5 atm; lines (solid lines: NUIG, dashed lines: JetSurF) are simulation and symbols are experiment. C_0 and C denote initial concentration of *n*-pentane and concentration of chemical species after shock heated. Effective heating times used at 1000, 1100, 1200, 1300, 1400 and 1500 K were 1820, 1750, 1670, 1600, 1500 and 1500 μs, respectively.

The concentration of *n*-pentane begins to decrease at 1100 K. The concentrations of propene (C_3H_6) and 1-butene (C_4H_8-1) increase with increasing temperature to approximately 1300 K and decrease thereafter. The concentration of propane (C_3H_8) increases until the temperature

reaches approximately 1350 K and then decreases at higher temperatures. The concentrations of methane (CH_4), ethane (C_2H_6), ethylene (C_2H_4), acetylene (C_2H_2), 1,3-butadiene (1,3-C_4H_6), allene (C_3H_4-a), propyne (C_3H_4-p) and 1-buten-3-yne (C_4H_4) simply increase as temperature rises under our experimental conditions. The concentration of 1,2-butadiene (1,2-C_4H_6) is very low from 1200 to 1500 K.

Both the NUIG and JetSurF (Version2.0) models basically capture well these species versus temperature profiles except the cases of methane, propane and propene in JetSurF (Version2.0). A reaction path analysis was carried out using the NUIG model for the shock tube conditions outlined in Fig. 2.

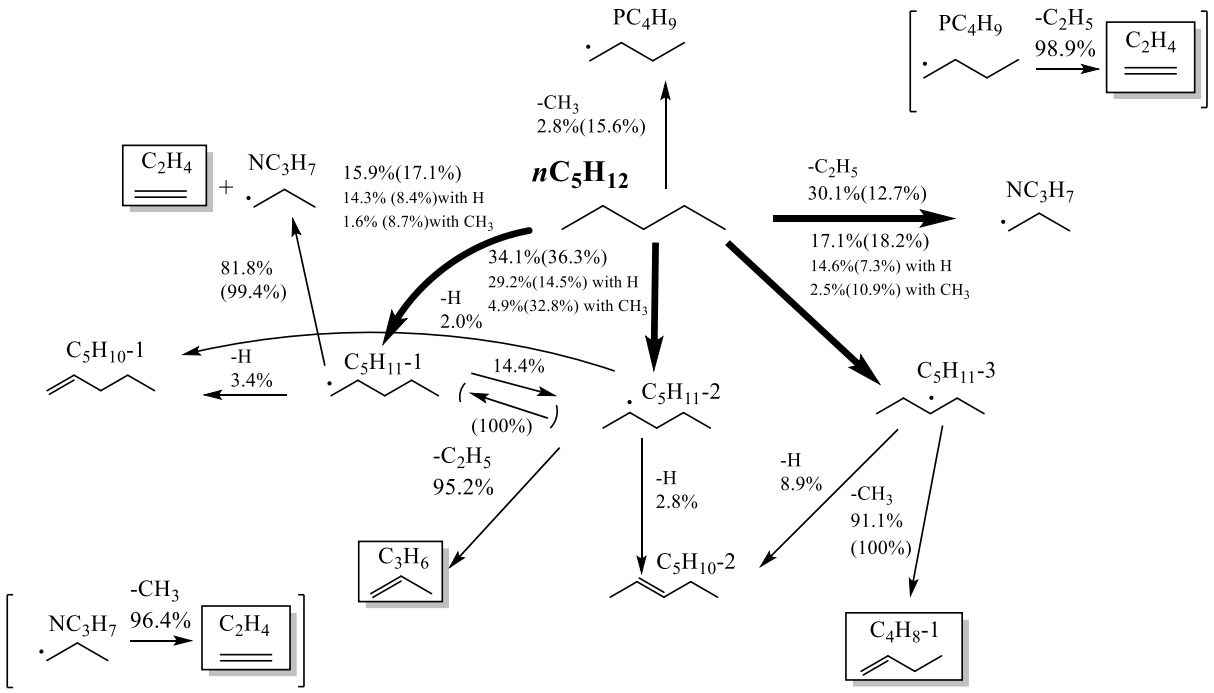

Fig. 2. Reaction path analysis for *n*-pentane pyrolysis. Shock condition; 1.6% *n*-pentane diluted in Ar, 1300 K 1.96 atm, approximately 20% consumption using NUIG model corresponding to 50 μs heating. The numbers with and without parenthesis are in the cases of JetSurF (version2.0) and NUIG, respectively.

The reaction scheme shows that *n*-pentane undergoes a simple C–C bond scission reactions to produce methyl and 1-butyl ($p\dot{C}_4H_9$) radicals, ethyl ($\dot{C}_2H_5$) and *n*-propyl ($n\dot{C}_3H_7$) radicals, and hydrogen ($\dot{H}$) atom abstraction reactions producing 1-pentyl ($\dot{C}_5H_{11}$-1), 2-pentyl ($\dot{C}_5H_{11}$-2) and 3-pentyl ($\dot{C}_5H_{11}$-3) radicals, which accounts for 2.8%, 30.1%, 15.9%, 34.1% and 17.1% of total *n*-pentane consumed, respectively. The *n*-propyl and 1-butyl radicals produced via simple C–C bond scission reactions undergo *β*-scission to form a methyl ($\dot{C}H_3$) radical and ethylene, an ethyl radical and ethylene, respectively. The 1-pentyl radical produced via hydrogen atom abstraction reactions undergoes isomerization and *β*-scission of C–C and C–H bonds to produce a 2-pentyl radical, a *n*-propyl radical and ethylene, 1-pentene (C_5H_{10}-1) and a hydrogen ($\dot{H}$) atom. The 2-pentyl radical produced via hydrogen atom abstraction reactions undergoes *β*-scission of C–C and C–H bonds to produce an ethyl radical and propene, 2-pentene (C_5H_{10}-2) and a hydrogen atom. The 3-pentyl radical produced via hydrogen atom abstraction reactions undergoes *β*-scission of C–C and C–H bonds to produce a methyl radical and 1-butene, 2-pentene and a hydrogen atom.

Ethylene is principally produced via unimolecular decomposition reactions of ethyl (–198), *n*-propyl (–492) and 1-pentyl (1114) radicals produced via the unimolecular decomposition reactions of *n*-pentane (1073), and 1- and 2-pentyl radicals (1114 and 1116).

Propene is mainly produced via the unimolecular decomposition of 2-pentyl radicals (1116) and principally decomposes via hydrogen atom abstraction reactions and hydrogen atom addition to the double bond of propene producing ethylene and a methyl radical (488).

Methane is mainly produced via hydrogen atom and methyl radical association reaction

(43) and hydrogen abstraction by methyl radical from hydrogen molecule (44), ethane (195), ethyl (201) radical, ethylene (226), propene (466) and *n*-pentane (1083), (1099) and (1100).

Ethane is produced via the recombination reaction (186) of methyl radicals, and is consumed via hydrogen abstraction reactions by hydrogen atoms (190) and methyl radicals (195).

Acetylene is mainly produced via unimolecular decomposition reactions of vinyl ($\dot{C}_2H_3$) radicals (–238) and 1-propen-1-yl ($\dot{C}_3H_5$-s) radicals (–608) produced via unimolecular decomposition reactions of 1-buten-4-yl ($\dot{C}_4H_7$1-4) radical (784), 1-penten-4-yl ($\dot{C}_5H_9$1-4) radical (–1192), 2-penten-5-yl ($\dot{C}_5H_9$2-5) radical (–1195), and hydrogen atom abstraction reactions by hydrogen atoms (222) (476) (477) and methyl (226) (482) radicals from ethylene and propene.

1-Butene is produced via unimolecular decomposition reactions of 3-pentyl radicals (1119) and is mainly consumed via hydrogen abstraction reactions and hydrogen atom addition to the double bond in 1-butene to produce ethylene and ethyl radicals (828) and propene and methyl radicals (829), and a hydrogen shift reaction (839) of 1-butene catalyzed by hydrogen atoms.

1,3-Butadiene is mainly produced via the β-scission reactions of 1-buten-3-yl ($\dot{C}_4H_7$1-3) (783), 1-buten-4-yl (785) and 1-penten-3-yl ($\dot{C}_5H_9$1-3) (–1190) radicals that are principally produced via hydrogen atom abstraction reactions from 1-butene and 1- and 2-pentene and unimolecular decomposition reaction of 2-pentene (C_5H_{10}-2) (–1141).

Propane is produced via the association reaction (–407) of methyl and ethyl radicals and

mainly decomposes via hydrogen abstraction reactions.

1-Buten-3-yne is produced via the decomposition of 1,3-butadien-1-yl ($\dot{C}_4H_5$-n) (–902) and 1,3-butadien-2-yl ($\dot{C}_4H_5$-i) (–903) radicals produced via hydrogen abstraction reactions from 1,3-butadiene.

1,2-Butadiene is mainly produced via the β-scission reactions of 1-buten-2-yl ($\dot{C}_4H_7$-12) (780) and 1-buten-3-yl (782) radicals. These radicals are produced via hydrogen abstraction reactions from 1- and 2-butene and unimolecular decomposition reaction (–1141) of 2-pentene.

Allene is principally produced via hydrogen abstraction by methyl (497) radicals from allyl radicals (produced from propene) and the β-scission reactions of allyl (–590) and 1-buten-2-yl (781) radicals.

Propyne is mainly produced via isomerization reaction of allene (564), the β-scission reactions of 1-propen-2-yl ($\dot{C}_3H_5$-t) (–597) (–598), allyl (–602) and 2-buten-2-yl ($C_4H_7$2-2) (788) radicals, and hydrogen shift reaction of allene (588) catalyzed by hydrogen atoms. 1-Propen-2-yl ($\dot{C}_3H_5$-t) and 2-buten-2-yl ($\dot{C}_4H_7$2-2) radicals are produced via hydrogen abstraction reactions from propene and 2-butene.

All of C_1–C_4 hydrocarbons mentioned above were detected except 2-butene. A carbon balance considering the species measured in the SPST experiments is compared to the simulations using the NUIG model, Fig. 3. The lowest measured carbon balance was 96% for the mixture containing 1.6% *n*-pentane diluted in Ar at 1.2–2.5 atm. The major undetected species predicted in the simulations are 1-pentene, 2-pentene and 2-butene

(C_4H_8-2), in which their predicted concentrations are less than 1% in the temperature range of study (1000–1500 K).

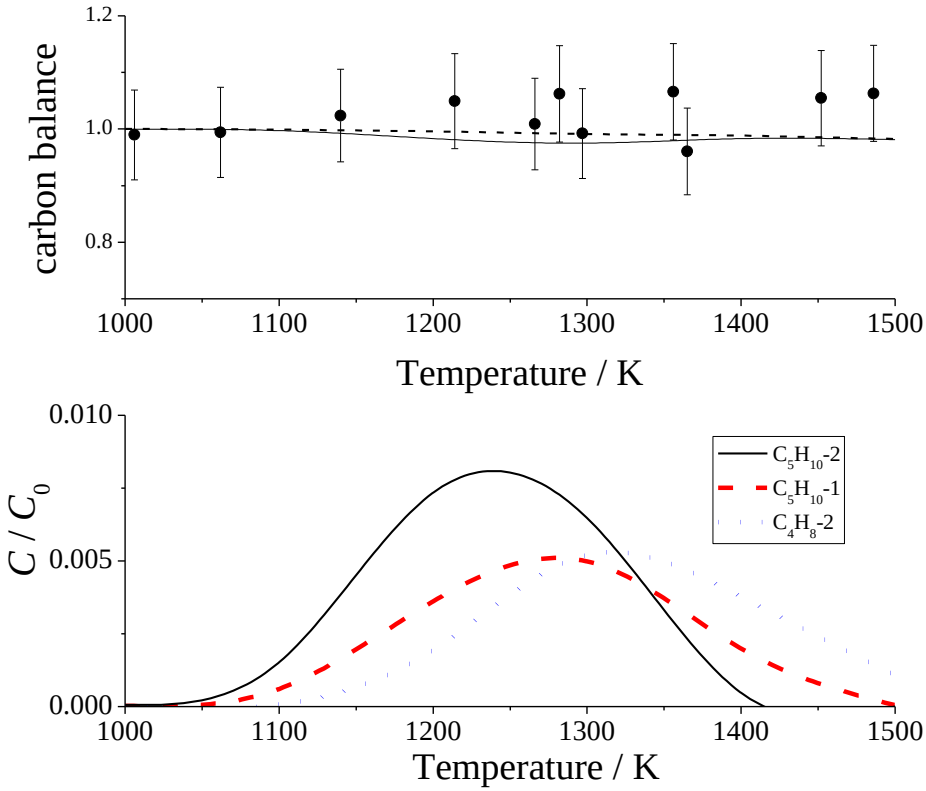

Fig. 3. Carbon balance measured in the SPST and simulated using the NUIG model for 1.6% *n*-pentane diluted in Ar at 1.2–2.5 atm; symbols are experimental results and lines are simulations. In the upper figure the solid line corresponds to the carbon balance considering species detected in the experiments, the dashed line includes the three compounds shown in the lower figure predicted in the simulation.

n-Hexane

The results from the *n*-hexane (*n*-C_6H_{14}) pyrolysis are shown in Fig. 4. The concentration of *n*-hexane begins to decrease at 1100 K. The concentration of 1-butene increases as the temperature rises to approximately 1200 K and then decreases.

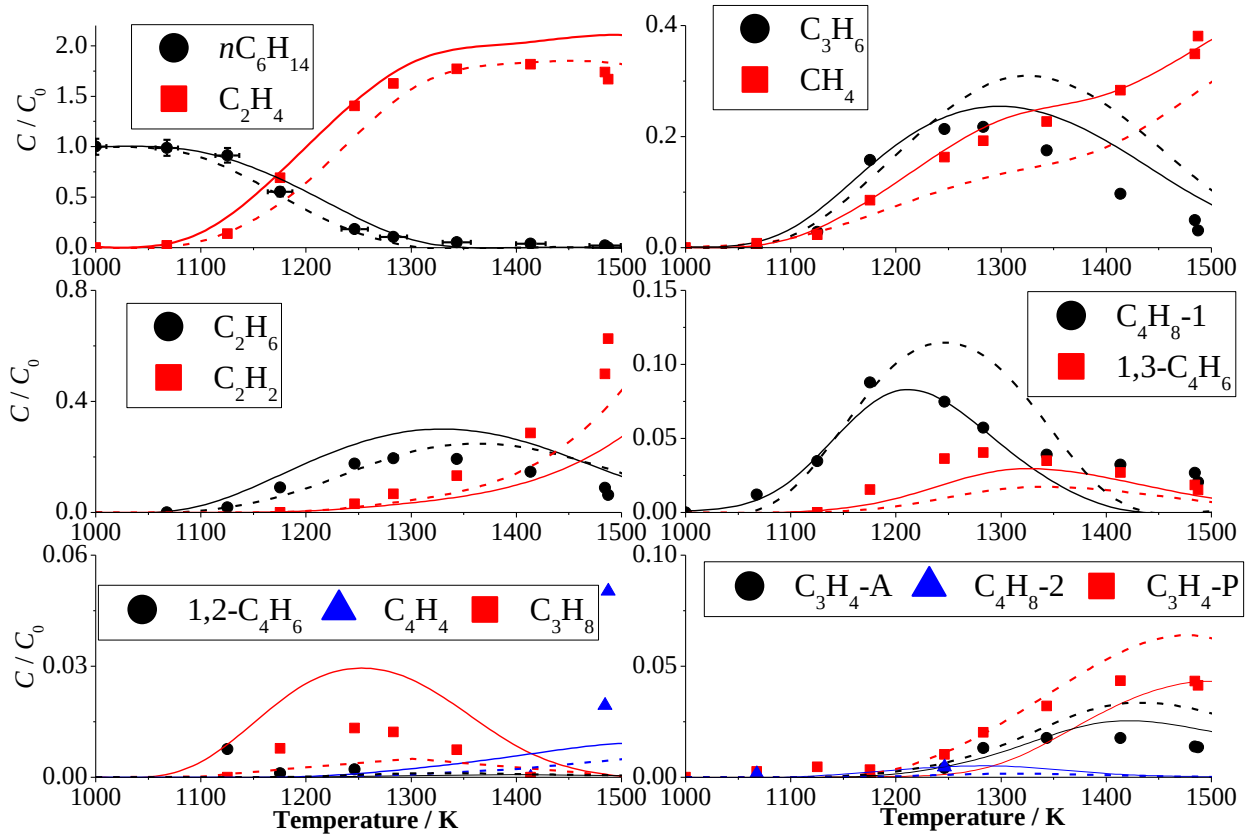

Fig. 4. Species profiles from SPST for 0.4% *n*-hexane diluted in Ar at 1.0–2.0 atm; lines (solid lines: NUIG, dashed lines: JetSurF) are simulation and symbols are experiment. C_0 and C denote initial concentration of *n*-hexane and concentration of chemical species after shock heated. Effective heating times used at 1000, 1100, 1200, 1300, 1400 and 1500 K were 2200, 2100, 2000, 1900, 1800 and 1700 μs, respectively.

The concentration of propane increases as the temperature rises to approximately 1250 K, and then decreases. The concentrations of ethane, propene and 1,3-butadiene increase as the temperature rises to approximately 1300 K and then decrease. The concentration of allene increases to a temperature of approximately 1400 K and then decreases. The concentrations of methane, ethylene, acetylene and propyne simply increase with temperature at our experimental conditions. 1-Buten-3-yne was detected only at high temperatures (~ 1500 K).

The concentration of 2-butene and 1,2-butadiene remains low in the temperature range 1100–1300 K. Both the NUIG and JetSurF (Version2.0) models basically capture these species versus temperature profiles well.

A reaction path analysis was carried out for the shock tube conditions outlined in Fig. 5.

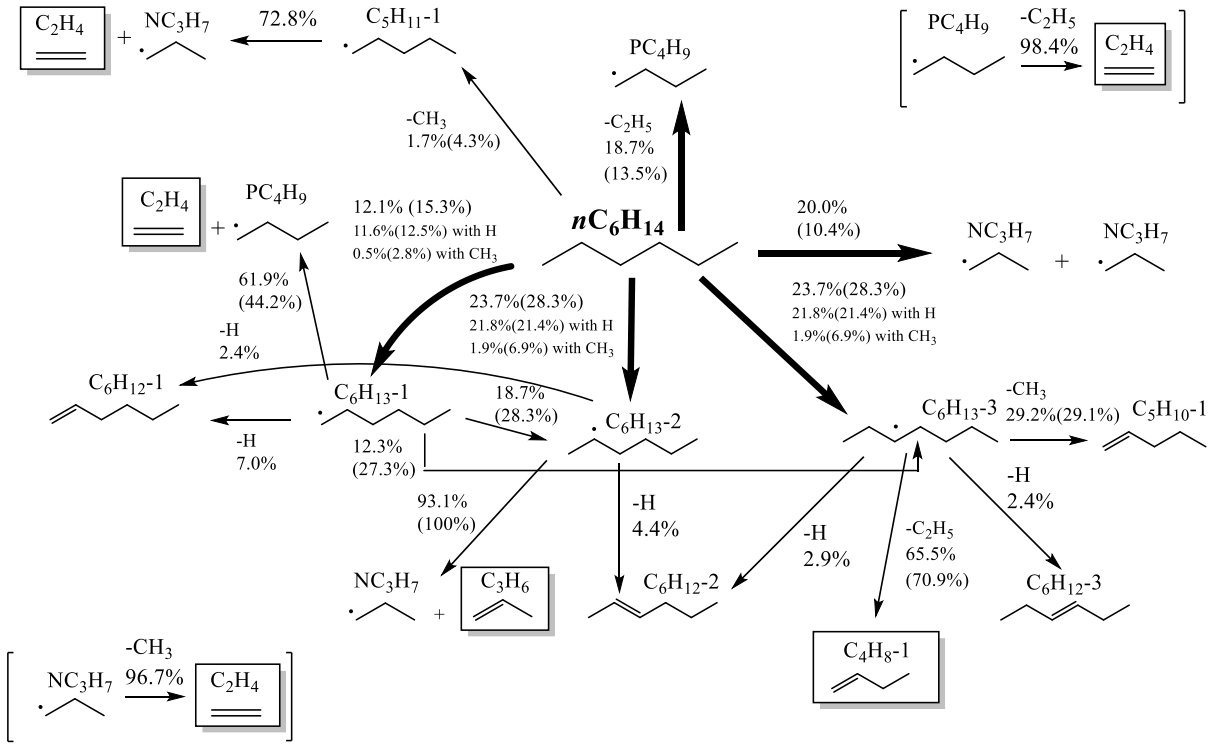

Fig. 5. Reaction path analysis for *n*-hexane shock pyrolysis. 0.4% *n*-hexane diluted in Ar, 1300 K 1.6 atm, approximately 20 % consumption using NUIG model corresponding to 30 μs heating. The numbers with and without parenthesis are in the cases of JetSurF (version2.0) and NUIG, respectively.

It is shown that *n*-hexane undergoes simple C–C bond scission reactions to produce methyl and 1-pentyl radicals, ethyl and 1-butyl radicals, and two *n*-propyl radicals, Fig. 5. Hydrogen atom abstraction reactions produce 1-, 2-, and 3-hexyl radicals, which accounts for 1.7%, 18.7%, 20.0%, 12.1%, 23.7% and 23.7% respectively, of the total *n*-hexane

consumed. Since the chemical reactions leading to the smaller products in *n*-hexane pyrolysis are fundamentally the same as those for *n*-pentane, only the reactions of hexyl radicals are discussed. 3-Hexyl ($\dot{C}_6H_{13}$-3) radicals isomerize to 2-hexyl ($\dot{C}_6H_{13}$-2) (1253) radicals and 1-hexyl ($\dot{C}_6H_{13}$-1) radicals (1254) via 5-membered and 6-membered transition state rings. 1-, 2-, and 3-hexyl radicals mainly decompose via β-scission to produce ethylene and 1-butyl radicals (1243), propyne and *n*-propyl radicals (1244), 1-butene and ethyl radicals (1245) and 1-pentene and methyl radicals (1246).

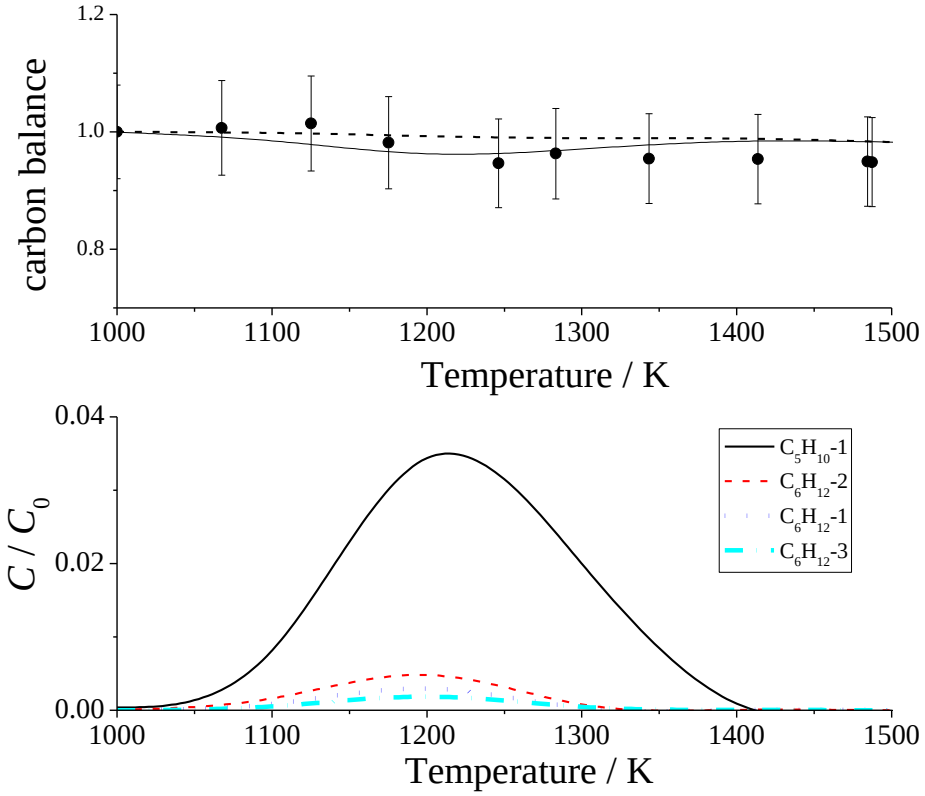

Fig. 6. Carbon balance from the SPST measurements and simulated species profiles using the NUIG model for 0.4% *n*-hexane diluted in Ar at 1.0–2.0 atm; symbols are experimental results and lines are simulations. In the upper figure the solid line indicates the carbon balance calculated for the experimentally detected species while the dashed line includes the four species shown in the lower figure predicted by the model in reasonable concentrations.

In the experiments 1-pentene was not detected, Fig. 6. The carbon balance from the SPST measurements is compared to the simulation using the NUIG model, Fig. 6. The lowest measured carbon balance was 94% for the mixture containing 0.4% *n*-hexane diluted in Ar at 1.0–2.0 atm. The major undetected species predicted in the simulation are 1-hexene (C_6H_{10}-1), 2-hexene (C_6H_{10}-2), 3-hexene (C_6H_{10}-3) and 1-pentene. The predicted concentrations of 1-, 2- and 3-hexene were less than 1% and that of 1-pentene was less than 4% in the temperature range of study (1000–1500 K).

***n*-Heptane**

The results from the *n*-heptane pyrolysis are shown in Fig. 7. The concentration of *n*-heptane begins to decrease at 1100 K. The concentration of 1-butene increases as the temperature rises to approximately 1300 K and then decreases. The concentrations of propane and propene increase as the temperature rises to approximately 1350 K and then decrease. The concentrations of methane, ethylene, ethane, acetylene, 1,3-butadiene, allene, propyne, 2-butene and 1-buten-3-yne simply increase as the temperature rises under our experimental conditions. The concentration of 1,2-butadiene remains low from 1100–1400 K. The NUIG model captures these species versus temperature profiles very well, while JetSurf (Version2.0) overestimates or underestimates the concentrations of 1-butene and propane.

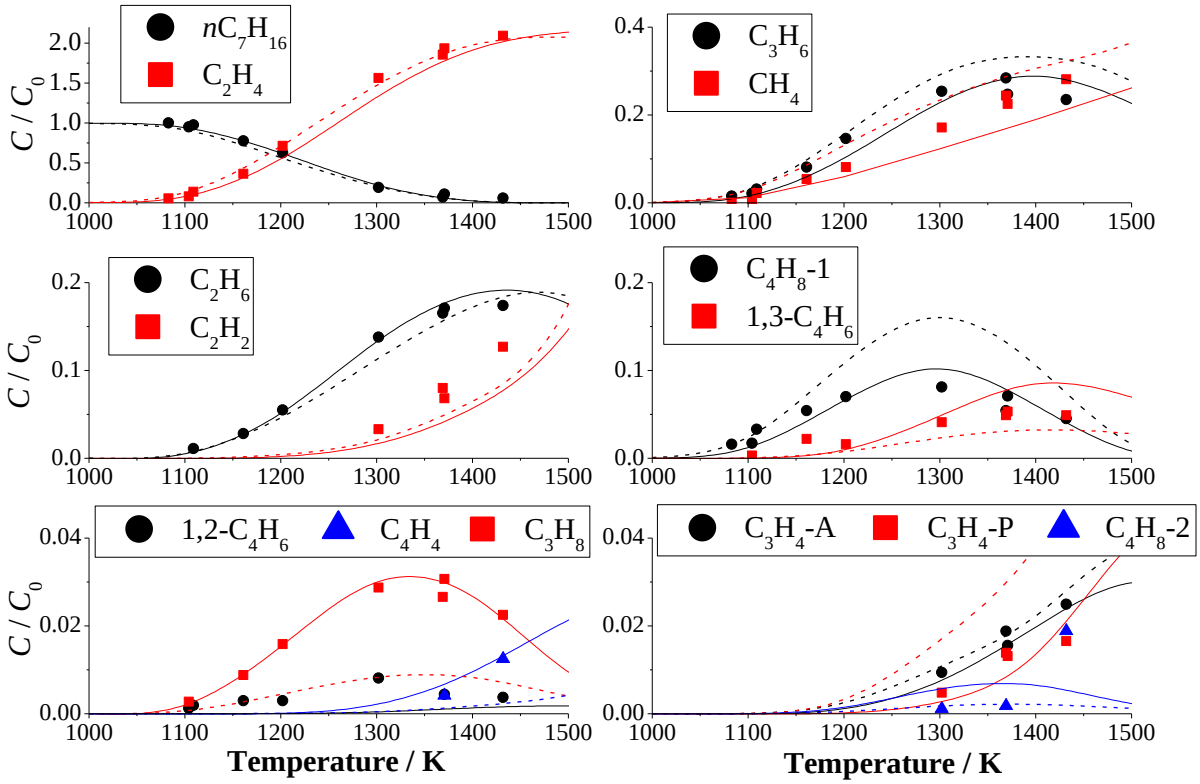

Fig. 7. Species profiles from SPST for 1.0% *n*-heptane diluted in Ar at 1.4-2.3 atm; lines (solid lines: NUIG, dashed lines: JetSurF) are simulation and symbols are experiment. C_0 and C denote initial concentration of *n*-heptane and concentration of chemical species after shock heated. Effective heating times used at 1000, 1100, 1200, 1300, 1400 and 1500 K were 2120, 2020, 1930, 1830, 1740 and 1640 μs, respectively.

A reaction path analysis was carried out for the shock tube conditions outlined in Fig. 8. The reaction scheme shows that *n*-heptane undergoes simple C–C bond scission reactions to produce methyl and 1-hexyl radicals, ethyl and 1-pentyl radicals, *n*-propyl and 1-butyl radicals, and hydrogen atom abstraction reactions producing 1-, 2-, 3- and 4-heptyl radicals, which accounts for 0.8%, 2.6%, 20.8%, 12.6%, 25.2%, 25.2% and 12.7% respectively, of the total *n*-heptane consumed. The *n*-propyl, 1-butyl, 1-pentyl and 1-hexyl radicals which are

among the major radicals generated in the *n*-pentane and *n*-hexane pyrolysis, undergo isomerization and β-scission of C–C and C–H bonds as described in the discussions of *n*-pentane and *n*-hexane pyrolysis presented earlier. The 1-heptyl (C_7H_{15}-1) radical produced via hydrogen atom abstraction undergoes isomerization and β-scission of C–C and C–H bonds to produce 2-heptyl (C_7H_{15}-2), 3-heptyl (C_7H_{15}-3) and 4-heptyl (C_7H_{15}-4) radicals, 1-pentyl radical and ethylene, and 1-heptene (C_7H_{14}-1) and a hydrogen atom. The 2-heptyl radical decomposes to produce a 1-butyl radical and propene, 1-heptene (C_7H_{14}-2) and a hydrogen atom, and 2-heptene (C_7H_{14}-2) and a hydrogen atom.

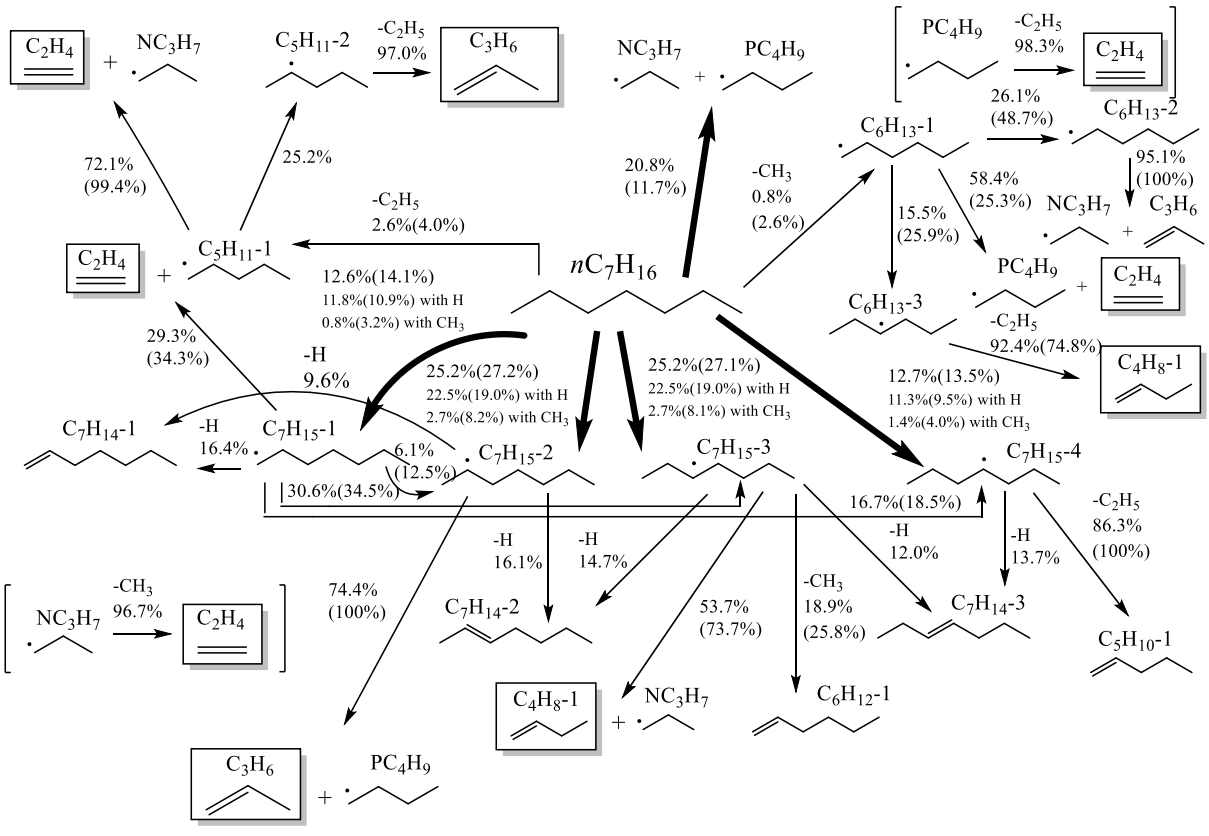

Fig. 8. Reaction path analysis for *n*-heptane pyrolysis. Shock condition; 1.0 % *n*-heptane diluted in Ar, 1300 K 1.96 atm, 20 % consumption using NUIG model corresponding to 45 μs heating. The numbers with and without parenthesis are in the cases of JetSurF (version2.0) and NUIG, respectively.

The 3-heptyl radical produces a methyl radical and 1-hexene, a *n*-propyl radical and 1-butene, 2-heptene and a hydrogen atom, and 3-heptene (C_7H_{14}-3) and a hydrogen atom. 27% of the 3-heptyl ($\dot{C}_7H_{15}$-3) radical is predicted to be consumed via C–H bond scission in the NUIG model. The branching ratio of the reaction producing 1-butene and *n*-propyl radical from 3-heptyl radicals decreases due to the contribution of simple C–H bond scission reactions, which affects the concentrations of 1-butene. The 4-heptyl radical produces a ethyl radical and 1-pentene, 3-heptene and a hydrogen atom. However, 1-hexene and 1-pentene were not detected, Fig. 9. The carbon balance measured in our SPST experiments is compared to that predicted using the NUIG model, Fig. 9. The lowest measured carbon balance was 91% for the mixture containing 1.0% *n*-heptane diluted in Ar at 1.4–2.3 atm. The major undetected species predicted are 1-, 2-, and 3-heptene 1-hexene, 1-pentene, 1,3-pentadiene and 1,2,4-pentatriene (C_5H_6). The predicted concentrations of most of these species are less than 3%, and that of 1-pentene was about 6% at 1300 K. However, it is anticipated that these concentrations are probably overestimated as the carbon balance is underestimated as shown in Fig. 9.

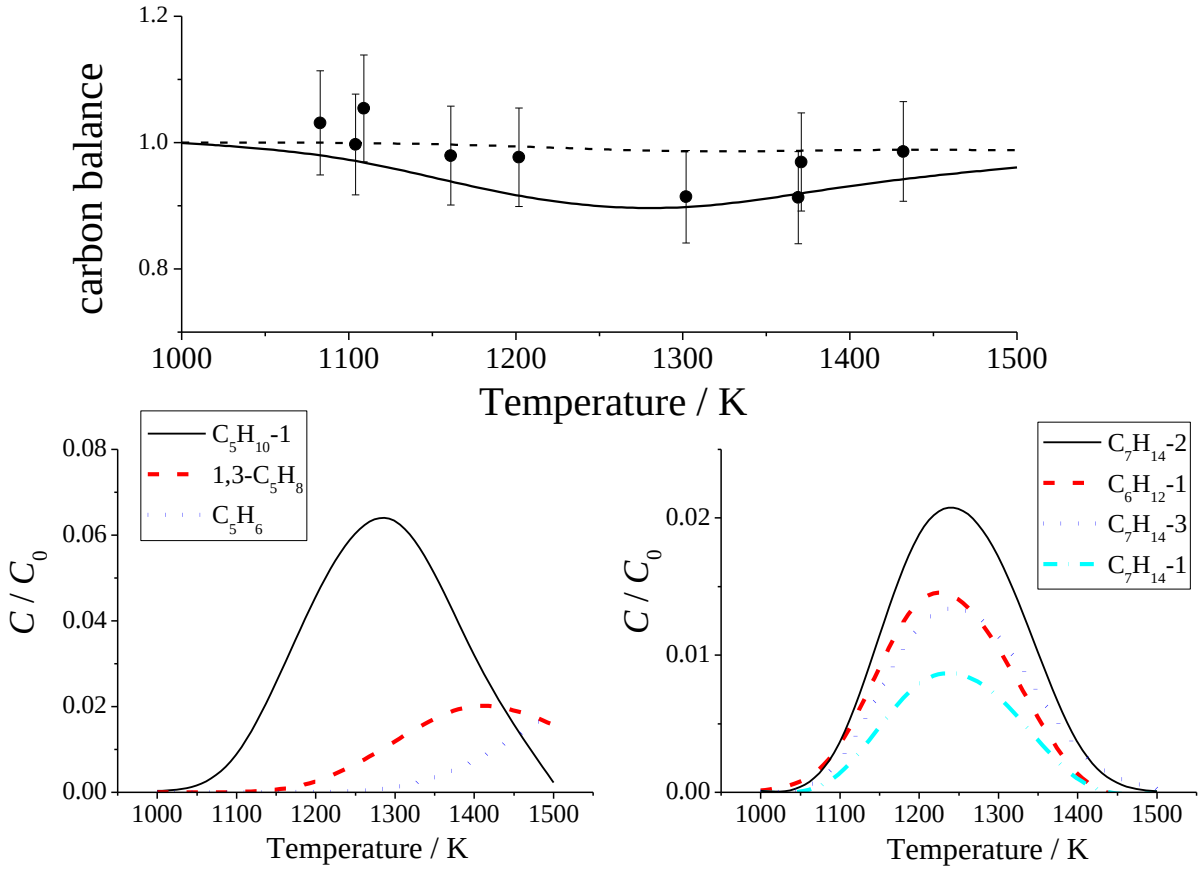

Fig. 9. Carbon balance from the SPST measurements and simulated using the NUIG model for 1.0% *n*-heptane diluted in Ar at 1.4–2.3 atm; symbols are experimental measurements and lines are simulations. In the upper figure, the solid line is the carbon balance calculated from species detected in the experiment while the dashed line includes the compounds that are shown in the lower figure which are predicted in reasonable concentration by the model.

Sensitivity Analyses

Sensitive analyses were carried out to investigate the dependence of the important reactions to the concentrations of *n*-pentane, *n*-hexane, *n*-heptane and products. The analysis was carried out by increasing both the forward and reverse rate constants by factors of 2 and 0.5, with sensitivities expressed using the formula: Sensitivity = (log (factor+/factor-))/(log

(k+/k-))) = (log (factor+/factor-))/(log (2/0.5)). Where, “factor” denotes concentrations of species. Figures 10–12 depict the sensitivity coefficients of species concentrations for 1.6% *n*-pentane at 1300 K, 1.96 atm and 1.6 ms, 0.4% *n*-hexane at 1200 K 1.41 atm 2.0 ms and 1.0 % *n*-heptane at 1300 K, 1.96 atm and 1.83 ms corresponding to the conditions presented in Figs. 1, 4 and 7. A positive sensitivity indicates an increase in species concentrations and conversely a negative value indicates a decrease in the species concentrations. Only those reactions which have sensitivity coefficients over 0.1 as absolute values are shown.

n-Pentane

Figure 10 depicts the sensitivity coefficients of species concentrations for 1.6% *n*-pentane at 1300 K, 1.96 atm and 1.6 ms. The C–C bond scission reaction of *n*-pentane producing ethyl and *n*-propyl radicals has a strong negative sensitivity on the concentration of *n*-pentane, while it has positive sensitivities on the concentrations of ethylene, ethane and propane. Hydrogen atom abstraction by hydrogen atoms from *n*-pentane at the central carbon producing 3-pentyl radicals has positive sensitivities on the ethane, 1-butene, and 1,2- and 1,3-butadiene concentrations. Hydrogen atom abstraction by hydrogen atoms from *n*-pentane producing 2-pentyl radicals shows a positive sensitivity on propene concentrations, while it has negative sensitivity to methane, ethane, 1,3-butadiene and 1,2-butadiene concentrations. Hydrogen atom abstraction by hydrogen atoms from *n*-pentane at primary carbon producing a 1-pentyl radical leads to a decrease in the concentrations of 1,3-butadiene and 1,2-butadiene. Hydrogen atom abstraction by methyl radicals from *n*-pentane at the central

carbon producing 3-pentyl radicals increases the concentrations of methane and 1-butene. Hydrogen atom abstraction by methyl radicals from *n*-pentane producing a 2-pentyl radicals leads to an increase in the concentrations of methane and propene, while it leads to a decrease in the concentration of ethane. The β-scission reaction of 3-pentyl radical producing a 1-butene and a methyl radical leads to a decrease in the concentrations of 1,3-butadiene. The β-scission of 3-, and 2-pentyl radicals producing 2-pentene and a hydrogen atom lead to an increase in the concentration of 1,3-butadiene, while the β-scission reaction of 2-pentyl radicals producing propene and ethyl radicals leads to a decrease in predictions of 1,3-butadiene. The rate constants for the primary reactions of *n*-pentane, which include unimolecular decomposition reactions of *n*-pentane and radicals derived from *n*-pentane, and hydrogen atom abstraction reactions from *n*-pentane have an influence on the concentrations of the species detected.

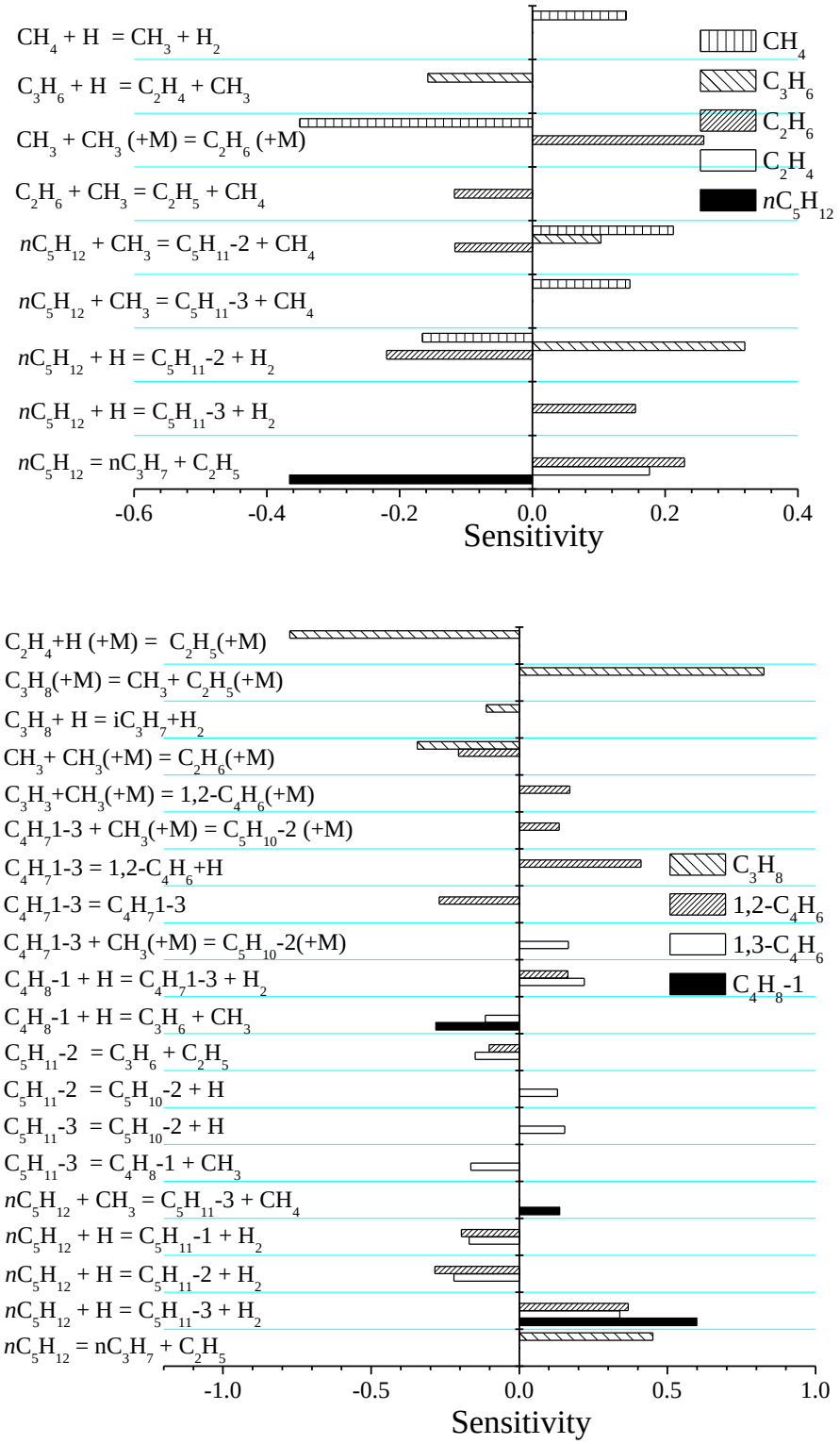

Fig. 10. Sensitivity to species concentration calculated with NUIG model; 1.6% *n*-pentane diluted in Ar, 1300 K, 1.96 atm, t_e = 1600 μs, corresponding to conditions in Figure 1.

***n*-Hexane**

Figure 11 depicts the sensitivity coefficients of species concentrations for 0.4% *n*-hexane at 1200 K, 1.41 atm 2.0 ms corresponding to the conditions presented in Fig. 4. The C–C bond scission reaction producing ethyl and 1-butyl radicals lead to a significant decrease in *n*-hexane concentration, while it increases the concentrations of ethylene, propene, 1-butene, 1,3-butadiene, 1,2-butadiene and propane. Hydrogen atom abstraction by hydrogen atoms from *n*-hexane producing 3-hexyl radical leads to a decrease in the concentrations of propene, while it leads to an increase in the concentrations of 1-butene, 1,3-butadiene, 1,2-butadiene and propane. Hydrogen atom abstraction by hydrogen atoms producing 2-hexyl radical leads to an increase in propene concentration, while it decreases the concentrations of 1-butene, 1,3-butadiene and 1,2-butadiene. Hydrogen atom abstraction by methyl radicals producing 3- and 2-hexyl radicals leads to an increase in methane concentration. The predicted concentrations of 1-butene and 1,2-butadiene are sensitive to the branching reaction of 3-hexyl radicals, while predictions of 1,3-butadiene and 1,2-butadiene are sensitive to the branching reaction of 2-hexyl radicals. The rate constants for the primary reactions of *n*-hexane, which include unimolecular decomposition reactions of *n*-hexane and radicals derived from *n*-hexane and hydrogen atom abstraction from *n*-hexane all have an influence on the concentrations of the species detected.

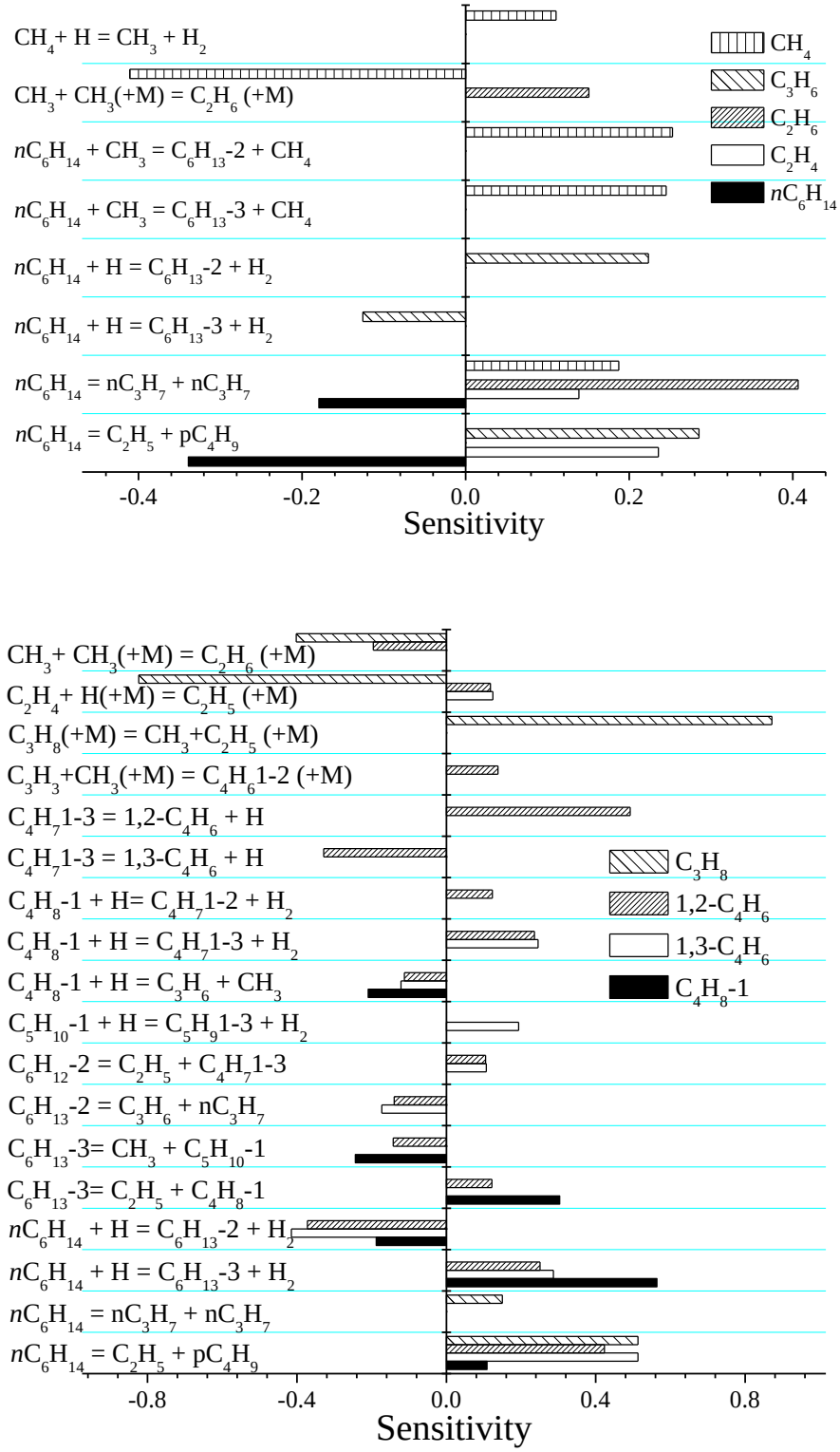

Fig. 11. Sensitivity to species concentrations calculated using the NUIG model; 0.4% *n*-hexane diluted in Ar, 1200 K, 1.41 atm, t_e = 2000 μs, corresponding to conditions in Figure 4.

n-Heptane

Figure 12 depicts the sensitivity coefficients of species concentrations for 1.0% *n*-heptane at 1300 K, 1.96 atm 1.83 ms corresponding to the conditions presented in Fig. 7. The C–C bond scission reaction of *n*-heptane producing 1-butyl and *n*-propyl radicals lead to a decrease in the concentrations of *n*-heptane and 1,2-butadiene, while it leads to an increase in the concentrations of ethylene, ethane and propane. Hydrogen atom abstraction by hydrogen atom from *n*-heptane producing 3-heptyl radicals also leads to a decrease in the concentration of *n*-heptane, while increasing the concentrations of ethane, 1-butene and 1,2-butadiene. Hydrogen atom abstraction by hydrogen atom producing 2-heptyl radicals leads to a decreases in the concentrations of *n*-heptane and ethane, while increasing propene concentrations. Hydrogen atom abstraction by methyl radicals from *n*-heptane producing 3-, and 2-heptyl radicals leads to an increase in methane concentrations. The β-scission reaction of 3-heptyl radicals producing *n*-propyl radicals and 1-butene leads to an increase in the concentrations of ethane and 1-butene. The predicted concentrations of propene, 1,3-butadiene and 1,2-butadiene are sensitive to the branching reaction of 2-heptyl radicals. The rate constants for the primary reactions of *n*-heptane, which include unimolecular decomposition reactions of *n*-heptane and radicals derived from *n*-heptane and hydrogen atom abstraction from *n*-heptane have an influence on the concentrations of the species detected.

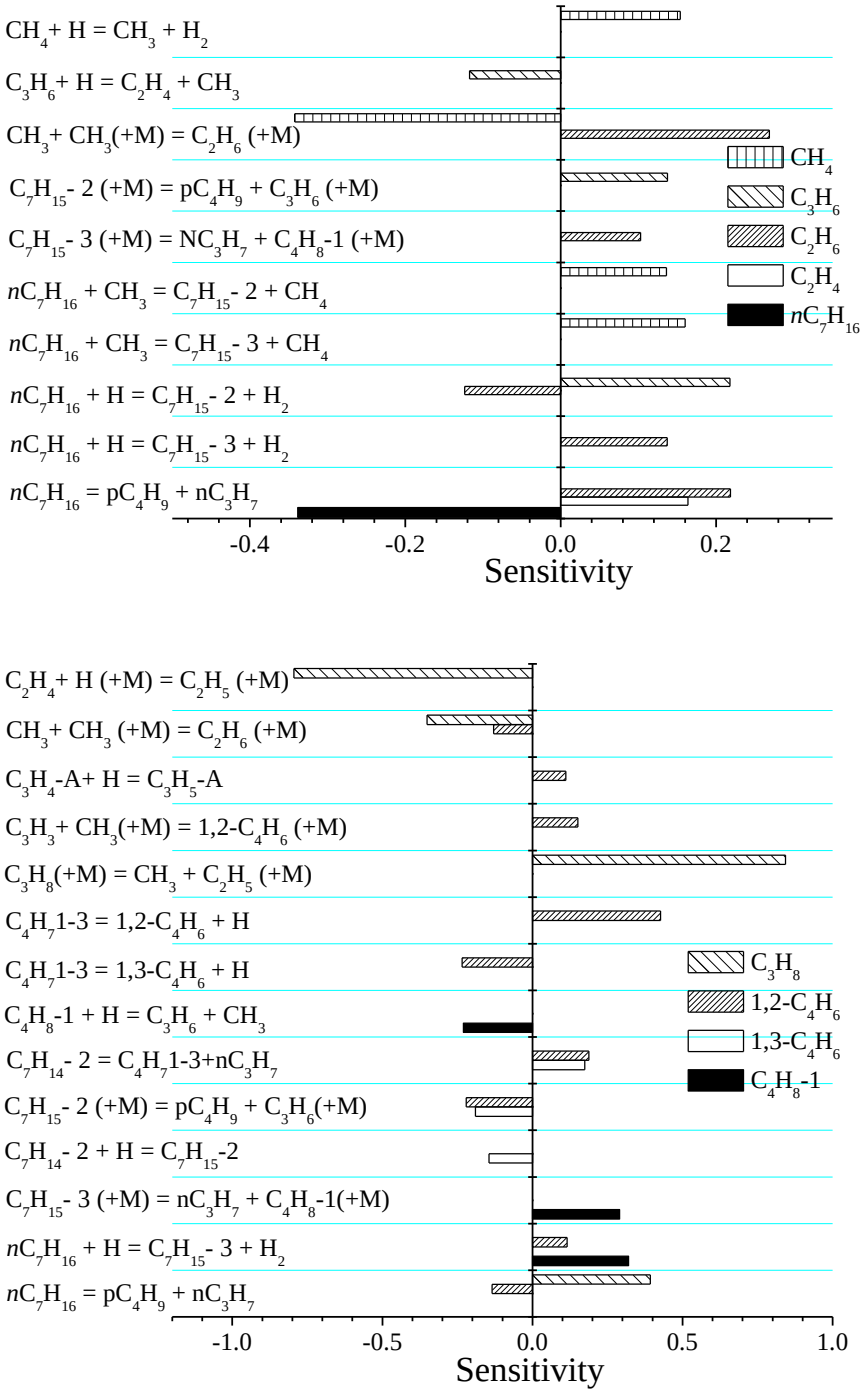

Fig. 12. Sensitivity to species concentration calculated with NUIG model; 1.0% *n*-heptane diluted in Ar, 1300 K, 1.96 atm, t_e = 1830 μs, corresponding to conditions in Figure 7.

Comparison of two models

The NUIG model is compared to JetSurF (version 2.0) for the conditions described in Figs. 1, 4 and 7. *n*-Pentane, *n*-hexane and *n*-heptane undergo simple C–C bond scission reactions

and hydrogen atom abstraction reactions by hydrogen atoms and methyl radicals in both models. The initiation reactions for fuel pyrolysis are the C–C bond scission reactions of reactants (*n*-pentane, *n*-hexane and *n*-heptane). The reactivities of *n*-pentane and *n*-hexane pyrolysis are higher in the cases of NUIG model. The total rates of unimolecular C–C bond scission reactions in NUIG model are higher by a factor of 2 in the cases of *n*-pentane and *n*-hexane, while it is similar (within 15%) in the case of *n*-heptane at 1300 K. The predictions using the NUIG model indicate that the fuel starts to decompose at lower temperatures in the cases of *n*-pentane and *n*-hexane relative to *n*-heptane because the C–C bond scission reactions have a strong influence to fuel consumption. JetSurF (version2.0) adopted faster rate constants for hydrogen atom abstraction reactions by methyl ($\dot{C}H_3$) radicals from *n*-pentane, *n*-hexane and *n*-heptane, while it has slower rates for the association reaction of methyl and ethyl radicals to produce propane. This explains the difference in predicted concentrations of propane and methane between the two models. 2-Pentyl radicals mainly decompose to produce an ethyl radical and propene in the NUIG model, while 100% of 2-pentyl radical isomerizes to 1-pentyl radical and then decomposes producing an *n*-propyl radical and ethylene in JetSurF (version2.0). The reactions of 2-pentyl radicals in JetSurf (version 2.0) seem to be anomalous. According to the work by Comandini et al. [29], who used a single pulse shock tube to measure ethylene and propene concentrations in the pyrolysis of 1-pentyl radicals, the 2-pentyl radical produced via isomerization of 1-pentyl radicals decomposed producing propene and an ethyl radical. Propene is produced via unimolecular decomposition of 2-pentyl radical as described above,

so the JetSurF (version 2.0) model underestimates the propene concentration as is shown in Fig. 1. All pentyl, hexyl and heptyl radicals undergo simple C–C and C–H bond scission reactions in the NUIG model, while C–H bond scission is not considered in JetSurF (version2.0).

4. Conclusions

The pyrolysis of *n*-pentane, *n*-hexane and *n*-heptane was studied in a single pulse shock tube. Species profiles of *n*-pentane, *n*-hexane, *n*-heptane, methane, ethane, ethylene, acetylene, propane, propene, allene, propyne, 1-butene, 2-butene, 1,3-butadiene, 1,2-butadiene as well as 1-buten-3-yne (C_4H_4) were obtained in the SPST using GC analysis at pressures of 1.0–2.5 atm and at effective heating times of 1.5–2.3 ms. Detailed chemical kinetic models from NUIG [8, 25, 26] and JetSurF (version 2.0) [28] were used to simulate these data. Simulations using both models explained the measured product concentration profiles well. Decomposition reactions for radicals such as pentyl, hexyl and heptyl radicals have a strong influence on the concentration profiles of the measured products. A carbon balance was also estimated for the pyrolysis of the three fuels, and was simulated using the NUIG model. The lowest measured carbon balance was 91% for *n*-heptane pyrolysis at 1302 K and 1369 K. Simulation using the NUIG model predicted the production of C_5–C_7 unsaturated hydrocarbons which mostly accounted for the missing carbon.

References

1. S. Tomioka, T. Hirakawa, T. Saito, K. Kato, M. Kodera, K. Tani, Transactions of the Japan Society for Aeronautical and Space Sciences, Aerospace Technology Japan 12 (2014) 91-98.
2. M. B. Sajid, T. Javed, A. Farooq, Shock tube/laser absorption measurements of methane, acetylene and ethylene during the pyrolysis of n-pentane and iso-pentane, Combust. Flame 164 (2016) 1-9.
3. C. K. Westbrook, W. J. Pitz, A kinetic modeling study of n-pentane oxidation in a well-stirred reactor, Combust. Flame 72 (1988) 45-62.
4. F. S. Gonzalez, S. Sandler, An experimental study of the oxidation of n-pentane in the high temperature pre-ignition region, Combust. Flame 26 (1976) 35-44.
5. R. Mével, K. Chatelain, P. A. Boettcher and J. E. Shepherd, Low temperature oxidation od n-hexane in a flow reactor, 8th US National Combustion Meeting, University of Utah, May 19-22, 2013, 070RK-0399.
6. Z. Wang, O. Herbinet, Z. Cheng, B. Husson, R. Fournet, F. Qi, F. Battin-Leclerc, Experimental investigation of the low temperature oxidation of the five isomers, J. Phys. Chem. A 118 (2014) 5573-5594.
7. F. Qi, Combustion chemistry probed by synchrotron VUV photoionization mass spectrometry, Proc. Combust. Inst. 34 (2013) 33-63.
8. K. Zhang, C. Banyon, C. Togbé, P. Dagaut, J. Bugler, H.J. Curran, An experimental and kinetic modeling study of n-hexane oxidation, Combust. Flame 162 (2015) 4194-4207.
9. A. Chakir, M. Bellimam, J. C. Boettner, M. Cathonnet, Kinetic study on n-heptane oxidation, Int. J. Chem. Kinet, 24 (1992) 385-410.
10. P. Dagaut, M. Reuillon, M. Cathonnet, High pressure oxidation of liquid fuels from low to high temperature. 1. n-heptane and iso-octane, Combust. Sci. Technol. 95 (1993) 233-260.
11. P. Dagaut, M. Reuillon, M. Cathonnet, Experimental study of the oxidation n-heptane in a jet stirred reactor from low to high temperature and pressures up to 40 atm, Combust. Flame 101 (1995) 132-140.

12. O. Herbinet, B. Husson, Z. Serinyel, M. Cord, V. Warth, R. Fournet, P. A. Glaude, B. Sirjean, F. Battin-Leclerc, Z. Wang. M. Xie, Z. Cheng, F. Qi, Experimental and modeling investigation of the low-temperature oxidation of *n*-heptane, Combust. Flame 159 (2012) 3455-3471.

13. H. M. Hakka, R. F. Cracknell, A. Pekalski, P. A. Glaude, F. Battin-Leclerc, Experimental and modeling study of ultra-rich oxidation of n-heptane, Fuel 144 (2015) 358-368.

14. C. V. Callahan, T. J. Held, F. L. Dryer, R. Minetti, M. Ribaucour, L. R. Sochet, T. Faravelli, P. Gaffuri, E. Rani, Experimental data and kinetic modeling of primary reference fuel mixtures, Proc. Combust. Inst. 26 (1996) 739-746.

15. T. Held, A. Marchese, F. Dryer, A semi-empirical reaction mechanism for n-heptane oxidation and pyrolysis, Combust. Sci. Technol. 123 (1997) 107-146.

16. D. B. Lenhert, D. L. Miller, N. P. Cernansky, K. G. Owens, The oxidation of a gasoline surrogate in the negative temperature coefficient region, Combust. Flame 156 (2009) 549-564.

17. T. J. Held, A. J. Marchese, F. L. Dryer, A semi-empirical reaction mechanism for *n*-heptane oxidation and pyrolysis, Combust. Sci. Technol. 123 (1997) 107-146.

18. C. Morley, Gaseq v0.79 <http://www.arcl02.dsl.pipex.com/gseqrite.htm>.

19. Y. Hidaka, S. Shiba, H. Takuma, M. Suga, Thermal decomposition of ethane in shock waves, Int. J. Chem. Kinet. 17 (1985) 441-453.

20. Y. Hidaka, T. Nakamura, A. Miyauchi, T. Shiraishi, H. Kawano, Thermal decomposition of propyne and allene in shock waves, Int. J. Chem. Kinet. 21 (1989) 643-666.

21. Y. Hidaka, K. Hattori, T. Okuno, K. Inami, T, Abe, T. Koike, Shock-tube and modeling study of acetylene pyrolysis and oxidation, Combust. Flame 107 (1996) 401-417.

22. Y. Hidaka, K. Kimura, K. Hattori, T. Okuno, Shock tube and Modeling Study of Ketene Oxidation, Combust. Flame 106 (1996) 155-167.

23. K. Yasunaga, R. S. Tranter, Speciation in Shock Tubes, in: F. Battin-Leclerc, J. M. Simmie, E. Blurock (Eds.), Cleaner Combustion, Springer-verlag, London, 2013, pp. 143-161.

24. CHEMKIN-PRO 15141, Reaction Design: San Diego, 2015

25. J. Bugler, B. Marks, O. Mathieu, R. Archuleta, A. Camou, C. Grègoire, K. A. Heufer, E. L. Petersen, H. J. Curran, An ignition delay time and chemical kinetic modeling study of the pentane isomers, Combust. Flame 163 (2016) 138-156.
26. K. Zhang, C. Banyon, J. Burgler, H. J. Curran, A. Rodriguez, O. Herbinet, F. Battin-Leclerc, C. B'Chir, K. A. Heufer, An updated experimental and kinetic modeling study of n-heptane oxidation, Combust. Flame 172 (2016) 116-135.
27. B. Sirjean, E. Dames, H. Wang, W. Tsang, Tunneling in hydrogen-transfer isomerization of n-alkyl radicals, J. Phys. Chem. A 116 (2012) 319-332.
28. H. Wang, E. Dames, B. Sirjean, D. A. Sheen, R. Tango, A. Violi, J. Y. Lai, F. N. Egolfopoulos, D. F. Davidson, R. K. Hanson, C. T. Bowman, C. K. Law, W. Tsang, N. P. Cernansky, D. L. Miller, R. P. Lindstedt, A high-temperature chemical kinetic model of *n*-alkane (up to *n*-dodecane), cyclohexane, and methyl-, ethyl, n-propyl and n-butyl-cyclohexane oxidation at high temperatures, JetSurF version 2.0, September 19, 2010 (http://web.stanford.edu/group/haiwanglab/JetsurF/JetSurF2.0/index.html).
29. A. Comandini, I. A. Awan, J. A. Manion, Thermal decomposition of 1-pentyl radicals at high pressures and temperatures, Chem. Phys. Lett. 552 (2012) 20-26.